Supplementary Table 1: Sequences of primers used for Real-time PCR.

Mcpt2	Forward 5′-ATTTCATTGCCTAGTTCCTCTGAC-3′
	Reverse 5′-CAGGATGAGAACAGGCTGGGAT-3′
Mcpt4	Forward 5′-GTAATTCCTCTGCCTCGTCCTTC-3′
	Reverse 5′-GTAATTCCTCTGCCTCGTCCTTC-3′
Mcpt6	Forward 5′-AGTAAGTGGCCCTGGCAGGTGAGCC-3′
	Reverse 5′-GGTCCCCATAGTATAGATACTGCTC-3′
Vegfa	Forward 5′-CACAGCAGATGTGAATGCAG-3′
	Reverse 5′-TTTACACGTCTGCGGATCTT-3′
Fgf2	Forward 5′- GAAACACTCTTCTGTAACACACTT-3′
	Reverse 5′- GTCAAACTACAACTCCAAGCAG-3′
Il6	Forward 5′-CTCTGGGAAATCGTGGAAAT-3′
	Reverse 5′-CCAGTTTGGTAGCATCCATC-3′
Col1a1	Forward 5′-CCTGGTAAAGATGGTGCC-3′
	Reverse 5′-CACCAGGTTCACCTTTCGCACC-3′
Tgfb1	Forward 5′-CAACAATTCCTGGCGTTACCTTGG-3′
	Reverse 5′-GAAAGCCCTGTATTCCGTCTCCTT-3′
Smad2	Forward 5′-ATGTCGTCCATCTTGCCATTC-3′
	Reverse 5′-AACCGTCCTGTTTTCTTTAGCTT-3′
Acta2	Forward 5′-CTGACAGAGGCACCACTGAA-3′
	Reverse 5′-CATCTCCAGAGTCCAGCACA-3′
Fn1	Forward 5′-CGAGGTGACAGAGACCACAA-3′
	Reverse 5′-CTGGAGTCAAGCCAGACACA-3′;
Smad2	Forward 5′-ATGTCGTCCATCTTGCCATTC-3′
	Reverse 5′-AACCGTCCTGTTTTCTTTAGCTT-3′
Smad7	Forward 5′-GGGCTTTCAGATTCCCAACTT-3′
	Reverse 5′-CACGCGAGTCTTCTCCTCC-3′
Bmp7	Forward 5′-CAAGCAGCGCAGCCAGAATCG-3′
	Reverse 5′-CAATGATCCAGTCCTGCCAGCCAA-3′;
Cdkn2a	Forward 5′-CCCCAGTGTCCTTACAGAGTG-3′
	Reverse 5′-GTGCCCAGAGTGGATGTCT-3′

Cdkn1a	Forward 5′-TGGT- GCTCATCCCTACCTTCA-3′
	Reverse 5′ -TTCTCTCTATCCTC TCCCCCAG-3′
Trp53	Forward 5′-TGTGTTCACCACACTAAGGGG-3′
	Reverse 5′-CCTTTGTTCTTGGCAGAAGACT-3′
Cdkn1c	Forward 5′-CTCAAGCTTCAAGATGTGGACCGTGCCAGT-3′
	Reverse 5′-GAGGAATTCGGGCGAGAACCTTCCAGAA-3′
Gadph	Forward 5′-AGCCACATCGCTCAGACAC-3′
	Reverse 5′-AGGCAGGTTTGATCTCCGTT-3′

Supplementary Figure and Figure legends

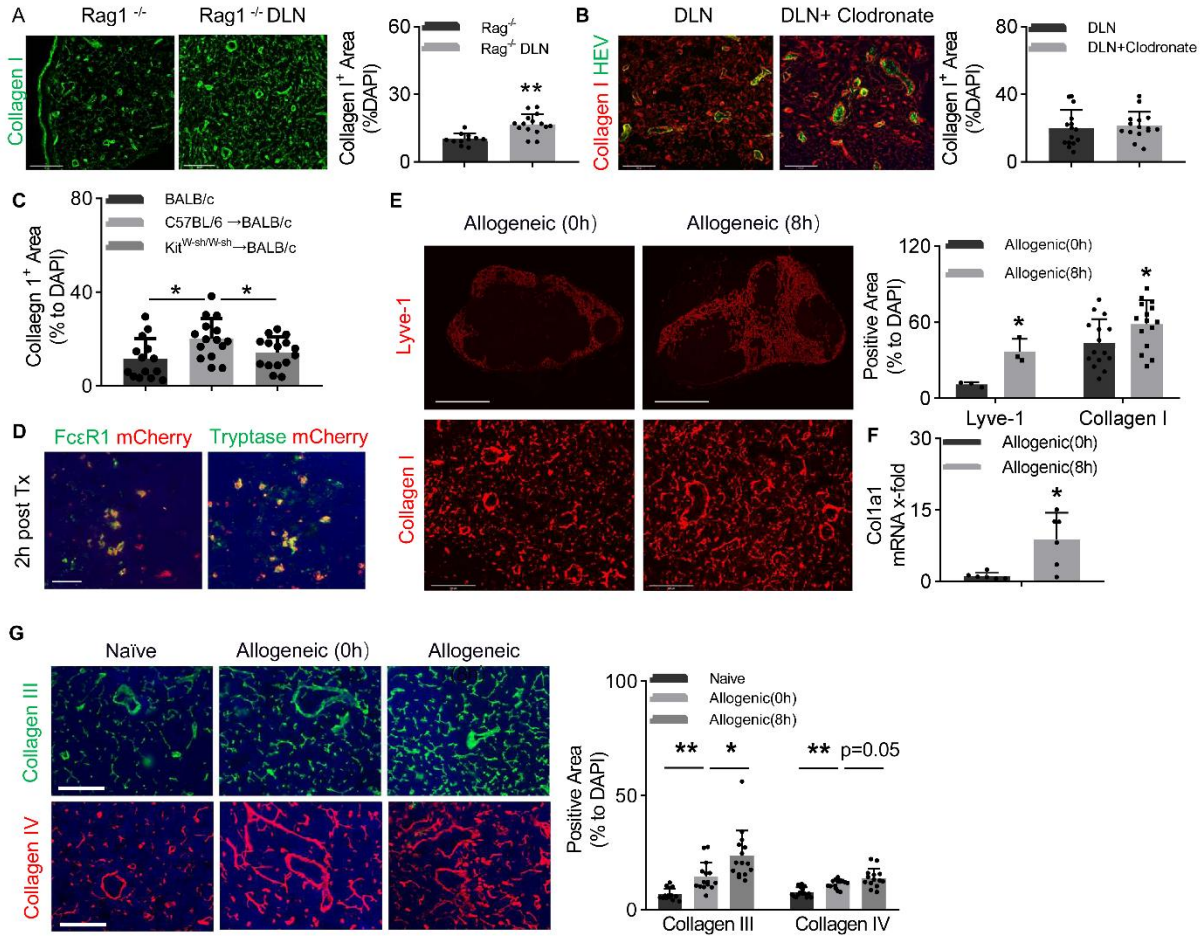

Supplementary Figure 1: Ischemia activates mast cell-induced collagen 1 accumulation and lymphangiogenesis in DLNs following skin transplantation. (A) Comparison and semi-

quantitative analysis of collagen I staining in DLNs from BALB/c → $Rag1^{-/-}$ skin transplant recipient mice in comparison to the axillary lymph nodes of $Rag1^{-/-}$ mice at day 1 after skin transplantation. Scale bar 100μm. (B) Comparison and analysis of collagen I staining and between DLNs of BALB/c→C57BL/6J skin transplant recipient mice with and without clodronate treatment. Scale bar 100μm. (C) Assessment of collagen 1^{+} region in the DLNs of naïve BALB/c mice, and those that received skin allografts from C57BL/6J and $Kit^{W\text{-}sh/W\text{-}sh}$ mice (n=4). (D) Fluorescence micrographs of DLNs of BALB/c recipients of skin allografts from C57BL/6-Tg(UBC–mCherry) donor mice demonstrate presence of mast cells within 2 hours following transplantation, as demonstrated by co-staining of the mast cell markers FcεR1 (green, left) and tryptase (green, right) with mCherry (red). (E) IF staining of Lyve-1^{+} lymphatic vessels and collagen 1^{+} region and semi-quantitative assessment in the DLNs following transplantation of WT and ischemic organs (~8 hours cold ischemia time, scale bars 1000μm and 100μm, n=4). (F) Gene expression level of *Col1a1* in the DLNs following transplantation of WT and ischemic organs (n=6). (G) Fluorescence micrographs and analysis of collagen III^{+} and collagen IV^{+} region in naïve LNs and DLNs following transplantation of WT and ischemic organs. Scale bars 50μm (n=3). Percentage of area stained positive in fluorescence micrographs was assessed in 3-6 random microscopic fields for each mouse. $*p < 0.05$; $**p < 0.01$ by Student's t test and 2-way ANOVA with Tukey's multiple-comparisons test.

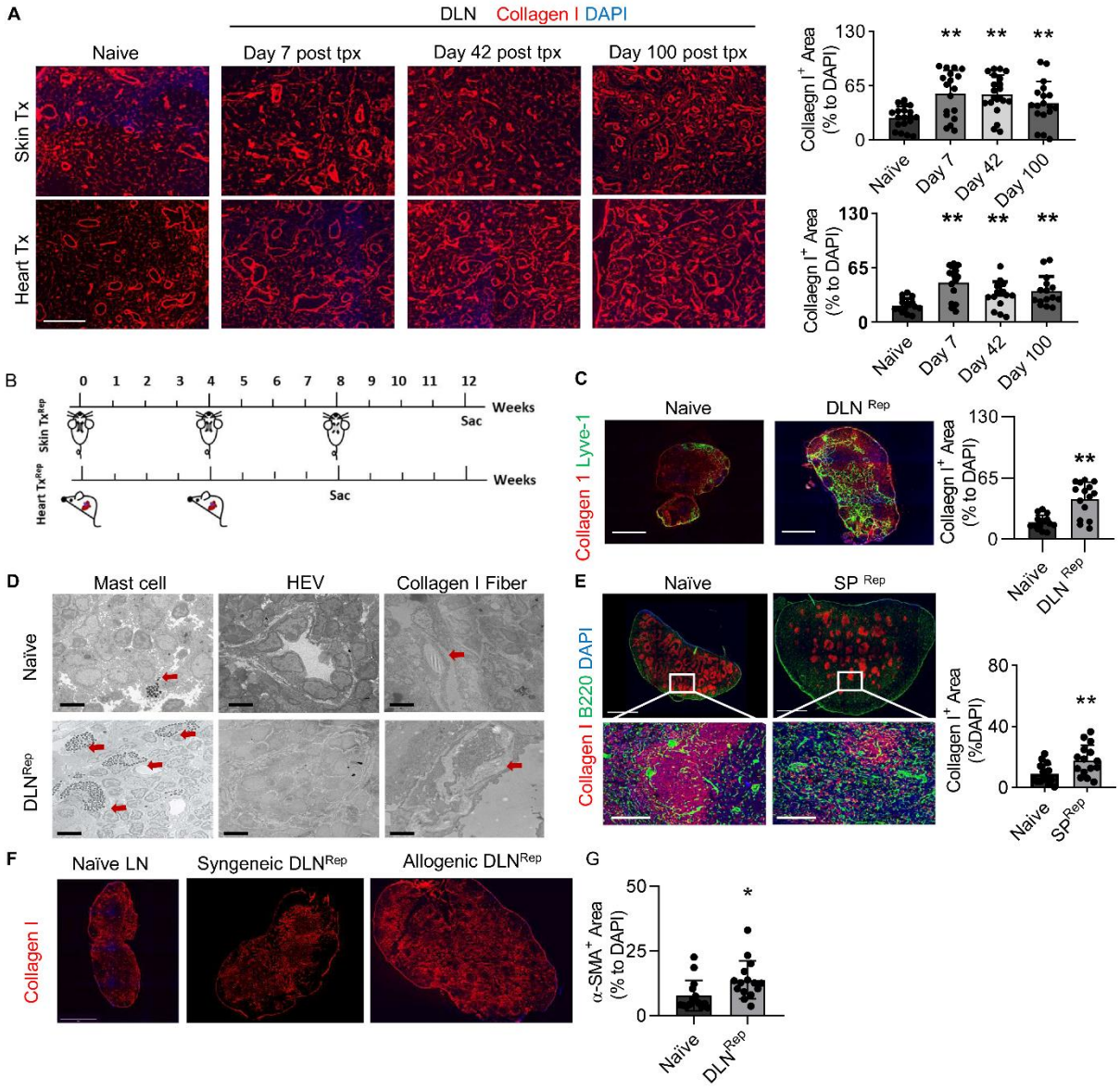

Supplementary Figure 2: Persistent accumulation of collagen 1 in DLNs following transplantation. (A) Fluorescence microscopic analysis shows marked increase of collagen 1 fibers (red) at 7, 42, and 100 days following skin and heart transplantation. Scale bar 100μm (n=3). (B) Schematic for the timelines of repetitive skin transplantation and heart transplantation models. (C) Fluorescence micrograph of collagen I^+ (red) and Lyve-1^+ (green) staining and semi-quantitative analysis of collagen 1^+ region in DLN^{Rep} following repetitive BALB/c → C57/BJ6 heart transplantation. Scale bar 1000μm (n=3). (D) Electron micrograph of one to two mast cells

located near lymphatics, HEVs, and collagen 1 fibers (red arrow) in naïve LN and higher number in DLN^{Rep}, along with obliteration of HEV lumen, detachment of HEV, and higher collagen 1 fiber density. Scale bar 2μm in mast cell and HEV images, 8μm in collagen 1 fiber images. (E) Fluorescence micrographs of collagen I^+ fibers (red) and $B220^+$ B cells (green) in the spleens of mice that underwent repetitive transplantation. Scale bars 1000μm and 50 μm (n=3). (F) Gene expression levels of collagen 1^+ (red) in LNs of naïve mice and DLN^{rep} of recipients of syngeneic and allogenic skin transplantation. Scale bar 1500μm. (G) Assessment of α-SMA^+ staining in naïve LNs and DLNs following repetitive skin transplantation. Scale bar 1000μm (n=4). Data in graphs are represented as means ± SD. Percentage of area stained positive in fluorescence micrographs was assessed in 3-6 random microscopic fields for each mouse. *$p < 0.05$; **$p < 0.01$ by Student's t test and 2-way ANOVA with Tukey's multiple-comparisons test.

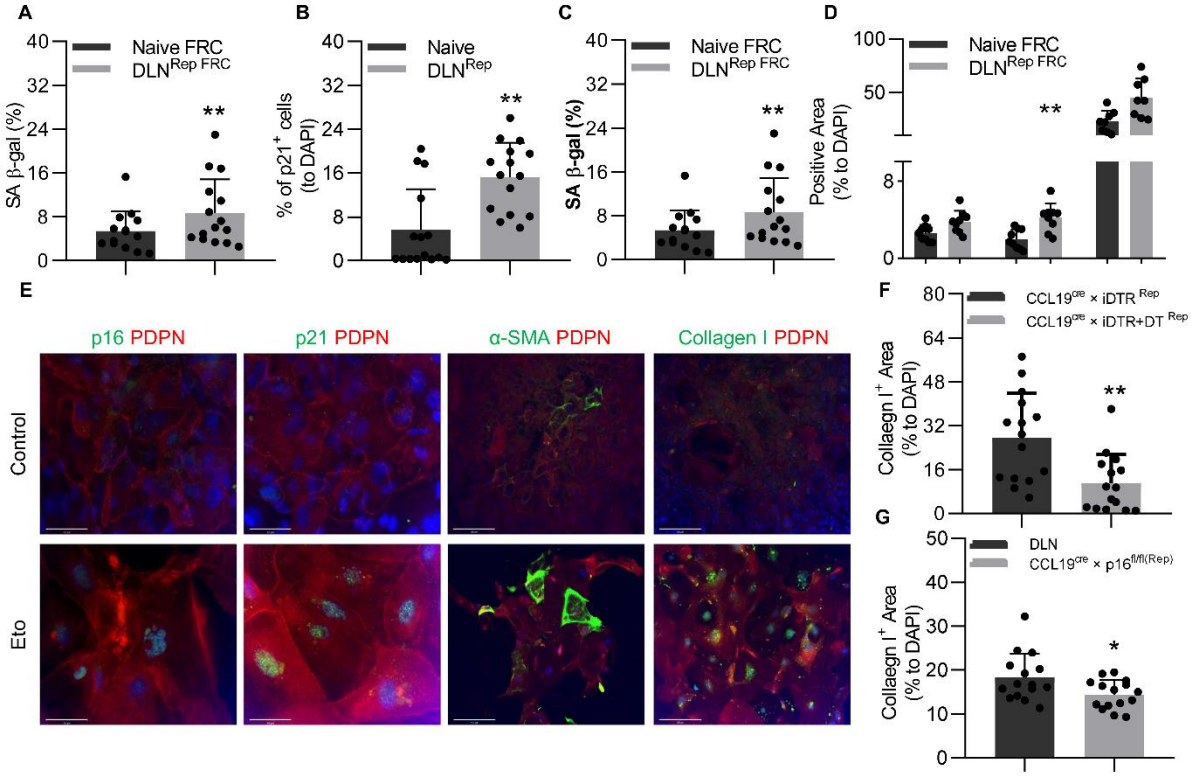

Supplementary Figure 3: Senescent FRCs promote fibrosis. Analysis of the percentage of (A) β-gal^{+} cells and (B) p21^{+} cells in naïve LNs and DLN^{Rep} (n=4). Analysis of (C) surface area percentage occupied by β-gal^{+} cells, and (D) α-SMA^{+}, collagen 1^{+}, and p21^{+} cells among FRCs isolated from naive LNs and DLN^{REP} (n=3). (E) IF staining shows that the expression levels of p16, p21, collagen 1, and α-SMA by cultured FRCs increase after etoposide treatment. Evaluation of collagen 1^{+} region in DLNs of (F) CCL19^{cre}×iDTR and (G) CCL19^{cre}×p16$^{fl/fl}$ allogeneic skin transplant recipients (n=4). Data in graphs are represented as means ± SD. Percentage of area stained positive in fluorescence micrographs was assessed in 3-6 random microscopic fields for each mouse. *$p < 0.05$; **$p < 0.01$ by Student's t test.

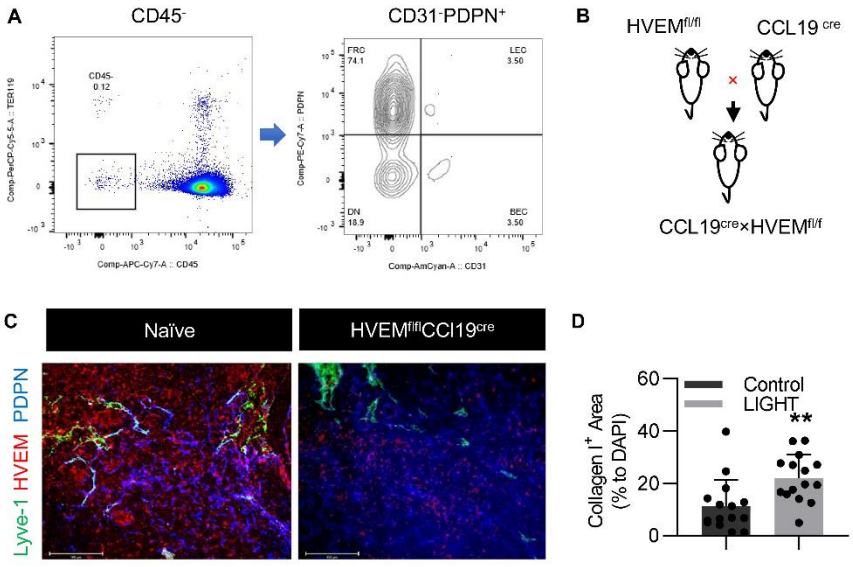

Supplementary Figure 4: HVEM expression in FRCs of C57BL/6J and CCL19^{cre}×HVEM$^{fl/fl}$ mice. (A) Gating strategy for flow cytometric analysis of FRCs. (B) Schematic for generation of CCL19^{cre} × HVEM$^{fl/fl}$ mice. (C) IF staining shows HVEM (red) expression by PDPN (blue)$^{+}$ LYVE-1(green)$^{-}$ FRCs. (D) Semi-quantitative analysis of collagen I^{+} fibers in naive (control) and LIGHT-treated FRCs (n=4). Data in graphs are represented as means ± SD. *$p < 0.05$; **$p < 0.01$ by Student's t test.

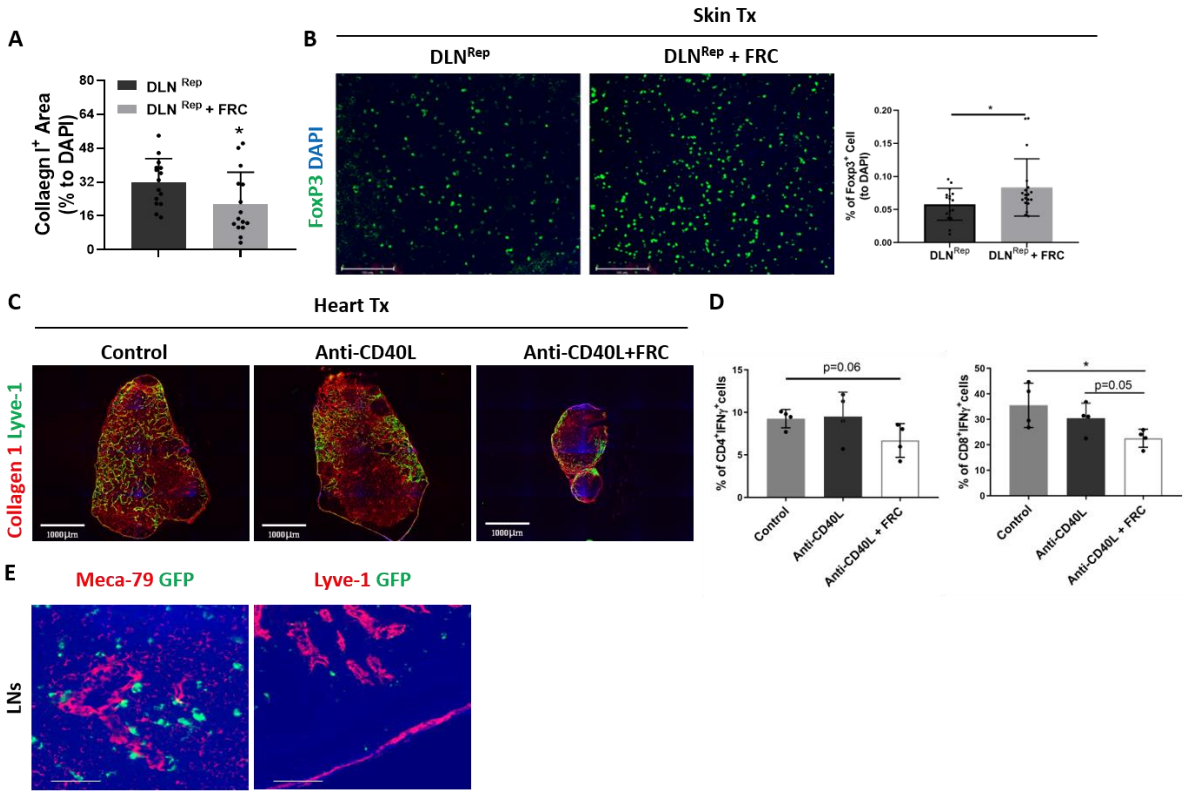

Supplementary Figure 5: FRC treatment improves immunosuppression post-transplantation. (A) Assessment of collagen I^+ staining in the DLNs of untreated mice (DLN^{Rep}) and mice treated with FRCs (DLN^{Rep} + FRC) (n=4). (B) IF staining of $Foxp3^+$ Tregs in DLN^{rep} from mice treated with and without FRCs. (C) Co-staining of LYVE-1 (green) and collagen 1 (red) in DLNs at 7 days after heart transplantation. Scale bar 1000µm. (D) Percentages of $CD4^+IFN\text{-}\gamma^+$ cells and $CD8^+IFN\gamma^+$ cells in splenocytes as measured by flow cytometry (each dot represents one biological replicate). (E) Fluorescence micrographs of DLNs of C57BL/6J mice harvested 24 hours following injection of CMFDA-FRCs. GFP signal was detected along with Meca-79^+ HEVs (Red) and Lyve-1^+ lymphatic vessels (Red). Data in graphs are represented as means ± SD. Percentage of area stained positive in fluorescence micrographs was assessed in 3-6 random microscopic fields for each mouse. $*p < 0.05$; $**p < 0.01$ by Student's t test and 2-way ANOVA with Tukey's multiple-comparisons test.